Korean J. Chem. Eng., **31**(8), 1480-1489 (2014)
DOI: 10.1007/s11814-014-0094-3

pISSN: 0256-1115
eISSN: 1975-7220

Influence of thermally induced, dehydroxylated nanoclay on polymer nanocomposites

Priyanka Pandey*, Smita Mohanty*,, and Sanjay Kumar Nayak*,**,†**

*Central Institute of Plastics Engineering and Technology (CIPET), Chennai, India
**Laboratory of Advanced Research in Polymeric Materials (LARPM), CIPET, Bhubaneswar, India
(*Received 17 December 2013 • accepted 27 March 2014*)

Abstract−This work reports a novel approach towards a chemical-free treatment of nanoclay through extensive thermal exposure. Dehydroxylation at high temperature was utilized to enhance the influence of nanoclay on the properties of polymer. The effect of this treatment of nanoclay, on the polymer properties, with reference to Polypropylene (PP) has been investigated. The FTIR spectra revealed the successful removal of water from the intergallery spacing of the nanoclay. The maintained structural configuration of the clay was confirmed using WAXD pattern. The uniform dispersion and exfoliation of thermally treated clay layers inside the polymer matrix was confirmed through enhanced mechanical properties. Improved crystallization properties, thermal stability and flame retardant characteristic were also noticed in the nanocomposites reinforced with thermally dehydroxylated clay. This study revealed that the dehydroxylation approach of modification of nanoclay may provide much enhanced properties of polymer, without involvement of any chemical for modification.

Keywords: Chemical Free, Thermal, Dehydroxylation, Mechanical Properties

INTRODUCTION

Polymer nanoclay hybrids have attracted considerable interest due to the dramatic enhancement in their physical, thermal and mechanical properties with relative to low required inorganic loading [1-8]. Wherein, this fact has already been established that in order to enhance the compatibility between clay and polymer the modification of nanoclay is necessary [8-10]. So as to render them compatible with most polymers and enlarge the basal spacing of clay to favor polymer intercalation, several approaches can be used to modify the clays, including adsorption, ion exchange, binding with inorganic and organic anions, grafting of organic compounds, reactions with acids, pillaring by different types of poly(hydroxometal) cations, interparticle and intraparticle polymerization, dehydroxylation and calcinations [11]. However, the approach of modification through dehydroxylation has not yet come into practice. Hence, our aim was to establish an approach to modify the polymer/nanoclay interface via dehydroxylation of nanoclay through thermal exposure slightly above its dehydroxylation temperature. By using this method, the exposure to by-products gases, evolved during processing of these polymer nanocomposites, using organophilic nanoclay can be avoided.

Polypropylene is a widely accepted polymer in many applications, so that the effort to optimize its properties via incorporation of nanofillers has been subject of scientific and industrial interest [12,13]. Further, the non-polar nature of polypropylene prevents the formation of interfacial interactions between macromolecular chain and clay layers; hence the requirement of incorporation of the polar group to the PP matrix, in the form of compatibilizer has already been reported earlier [14-16]. The use of Maleic anhydride grafted Polypropylene (MAPP) is the most preferred compatibilizer for this purpose [17-19]. These graft polymers of PP act as diluents of viscosity to plasticize the PP matrix and as interface modifiers to enhance the interfacial interaction in PP/inorganic filler composites [20].

In the present investigation, the influence of dehydroxylated nanoclay (through extensive thermal exposure) on the properties of polymer matrix was studied and reported. To understand the feasibility and validity of this modification, various properties of the nanocomposites, prepared via melt intercalation technique, were investigated. The mechanical properties of the PP and its nanocomposites were investigated to determine the uniformity/non-uniformity of dispersion of nanolayers inside the PP matrix. Further, to support this observation the crystallization property and nucleating effect was also investigated using differential scanning calorimeter and optical microscopic analysis. The thermal stability of polymer nanocomposites was also investigated by thermogravimetric analysis (TGA). The level of intercalation and exfoliation was analyzed through TEM micrographs.

MATERIALS

Polypropylene was procured from M/s Haldia Petrochemicals, Kolkata, India, having a density of 0.94 g/cm^3. The unmodified sodium montmorillonite nanoclay (Na-MMT) was purchased from Southern clay products, USA, having a diameter of about 40-60 nm. The compatibilizer used in this study was maleic anhydride grafted polypropylene (MAPP), OPTIM-P425, having a density 0.91 g/cm^3 was purchased from M/s Pluss Polymers Pvt. Ltd., Haryana, India.

EXPERIMENTAL

1. Surface Modification Montmorillonite Nanoclay

1-1. Thermal Treatment of Na-MMT

The Na-MMT was thermally treated via extensive heating of clay

†To whom correspondence should be addressed.
E-mail: papers.journal@gmail.com

at a temperature above dehydroxylation. Heating the clay to a temperature below dehydroxylation temperature and above dehydration temperature leads to loss of adsorbed and hydration water, resulting in collapse of the interlayer spaces. However, heating of the clay above dehydroxylation temperature (700 °C) leads to the exfoliation of Na-MMT by destroying its layered structure [21]. However, at 1,000 °C, tetrahedral sheets break down and a partial segregation of amorphous SiO_2 occurs. Therefore, the temperature for thermal treatment was selected above dehydroxylation temperature (>700 °C) and below 1,000 °C (i.e., 800 °C). The Na-MMT was kept at 800 °C for 1 hour, followed by sudden cooling at room temperature. The thermally treated clay is represented as TMMT in further discussion.

2. Fabrication of Nanocomposites

The single step mixing method was adopted to fabricate the nanocomposites using micro injection molding technique. The PP, MAPP and Na-MMT clay was compounded using microcompounder M/s DSM explore, Netherlands, (micro 15), at a temperature of 180, 185 and 185 °C in front, middle and rare zone, respectively, for 20 minutes with a 60 rpm of screw speed.

3. Fourier Transform Infrared Spectroscopy (FTIR)

Successful modification of Na-MMT, was confirmed through Fourier transform infrared spectroscopy (FTIR), Thermo scientific FTIR (smart orbit ATR 400-4,000 cm^{-1} with microscope). The heat dried samples of treated clays were used for analysis.

4. Wide Angle X-ray Diffraction (WAXD)

Wide angle x-ray diffraction (WAXD) analysis was used to analyze the interlayer gallery spacing of nanoclays and nanoclays in the polymer nanocomposites, using Philips X'Pert MPD (Japan), with graphite monochromator and a Cu Kα radiation source operated at 40 kv and 30 mA. An x-ray radiation source having wavelength of 1.54 A^0 (copper Kα_1, Ni filter), aperture slit of width 0.1 mm, and the scanning rate of 0.01 degrees per/s over the range of $2^0<2\theta<80^0$ (for clay) and $2^0<2\theta<30^0$ (PP and its nanocomposites) was used.

5. Mechanical Properties

Tensile properties of PP and modified clay reinforced nanocomposites were determined using Universal Tensile Machine (3382 Instron, UK) as per ASTM D 638. Five specimens of a dimension 127×12.7×3 mm^3 were subjected to tensile test at a gauge length of 50 mm and a speed of 5 mm/min. The Izod impact strength of the samples was also investigated using Tinius Olsen, USA, Impactometer, as per ASTM D256. The "V" notched samples were used for the analysis.

6. Heat Deflection Temperature (HDT)

The HDT tester, GOTECH HV 2000 C-3, was used to evaluate the heat deflection temperature of the PP and its nanocomposites. The samples were tested as per ASTM D 648.

7. Differential Scanning Calorimetry (DSC)

Differential scanning calorimetry (DSC) measurement was done by scanning the sample (about 10 mg), from −50 to 300 °C with a heating rate of 10 °C/min under nitrogen atmosphere using Q 20 series of TA instrument.

8. Thermogravimetric Analysis (TGA)

The thermal degradation temperatures and thermal stability of the PP and its nanocomposites were studied using a thermogravimetric analyzer (Q50 M/s TA instrument, USA). Samples of 10 mg were heated from 50 to 680 °C at a heating rate of 10 °C/min, and the corresponding initial, maximum and final degradation temperature were calculated.

9. Optical Microscopic Analysis

The spherulitic morphology of the PP its nanocomposites was investigated by using an optical microscope DM 4500, Leica Germany. A real-time observation of crystallization process and spherulite growth was performed by using a CCD color camera linked with polarized optical microscope (POM) in constant intervals. The samples were sandwiched and melted between two microscope cover slips for observation. The sample was melted in two steps. First, it was heated to 100 °C with a heating rate of 30 °C/min followed by heating to 200 °C with a rate of 20 °C/min in order to erase the thermomechanical history. The sample was kept for 5 minutes at this temperature to ensure complete melting. Further, to investigate the spherulitic structure the sample was allowed to cool and crystallized at given temperature with a rate of 10 °C/min to a temperature of 150 with an isotherm of 10 min. Further cooling was carried out with a lower rate of 3 °C/min to the room temperature. The morphologies were recorded at constant time intervals.

10. Transmission Electron Microscopy (TEM)

TEM analysis was carried out using a transmission electron microscope (JEOL 1200EX, Japan). The samples were microtomed under Cryo conditions, using a Leica EM UC6 microtome (M/s Leica, Germany). Sections having a thickness of 50 nm were collected from the water on a 300 mesh carbon-coated copper grids. TEM imaging was carried out at an accelerating voltage of 100 kV. Images were captured using a charged couple detector (CCD) camera for further analysis using Gatan Digital Micrograph analysis software.

11. Cone Calorimeter Analysis

The combustion analysis of the samples was carried out through the cone calorimeter experiments. The tests were carried out at 50 kW/m^2 heat fluxes with horizontal orientation of the samples (with a dimensions 100 mm×100 mm×3 mm) according to ASTM E 1354 by using a FTT cone calorimeter, Dual cone fire testing technology, UK.

12. Scanning Electron Microscope (SEM)

Scanning electron microscope was conducted with EVO MA 15 Germany, scanning electron microscope. The samples were prepared by gold coating before analysis. The filament voltage was set at 10-30 KV to make an image of the nanostructure.

RESULTS AND DISCUSSION

1. Fourier Transform Infrared Spectroscopy (FTIR)

FTIR spectra of unmodified and modified nanoclays are represented in Fig. 1. Both the clays revealed three characteristic absorption bands in its spectrum. The first absorption band below 600 cm^{-1} belongs to the bending vibration of S-O-Si, bridges. A second region of 800-950 cm^{-1} shows bending vibration of OH group, and the third absorption band at 1,030-1,250 cm^{-1} represents stretching vibration of Si-O-Si band. Following three similar regions were clearly visible from the FTIR spectrum of all the three clays (Na-MMT, TMMT) [22].

A diminished absorption band near 3,000-3,800 cm^{-1} in spectra of TMMT was noticed, revealing the dehydration of clay (montmorillonite) due to heating. However, the presence of characteristic

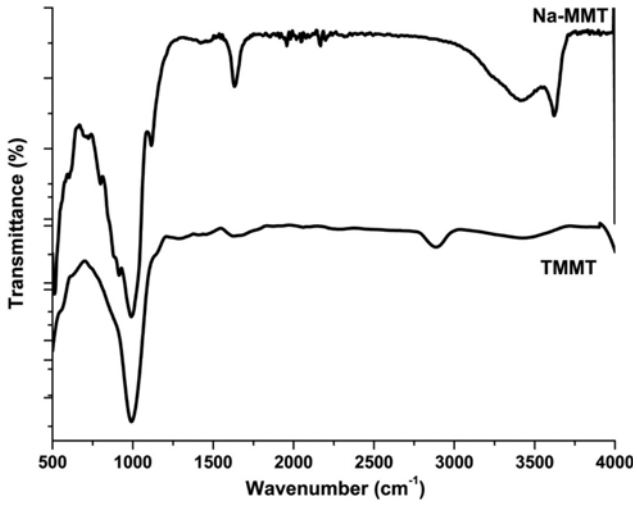

Fig. 1. FTIR spectrum of untreated and treated nanoclay.

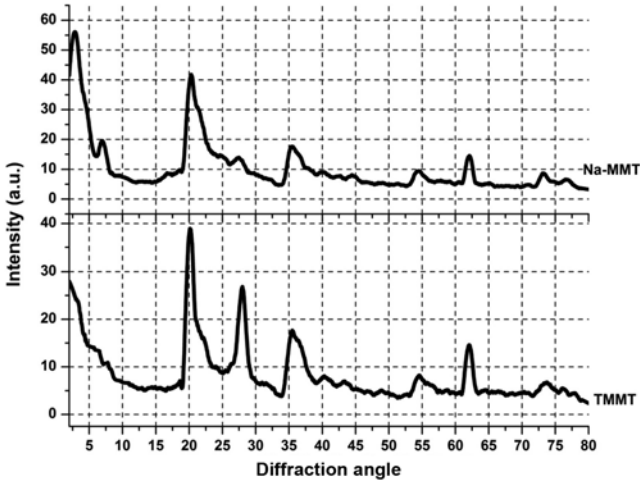

Fig. 2. XRD pattern of untreated and treated nanoclay.

peaks of clay (montmorillonite) revealed the maintained chemical characteristics of clay after thermal exposure above dehydroxylation temperature.

2. X-ray Diffraction Analysis (XRD)

Fig. 2 represents the XRD spectra of Na-MMT and TMMT nanoclay. From the spectra it was noticed that the peak corresponding to the intergallery spacing (d_{001}) almost disappeared, in case of TMMT, confirming the exfoliation of TMMT clay layers. This exfoliated morphology is attributed to the steam buildup between clay layers, which gets developed during heating, leading to the exfoliation of clay layers in the direction perpendicular to the layers [21]. Hence, it can be concluded that TMMT clay does not exhibit any ordered arrangement. This is probably due to the breakdown of the layered structure of clay mineral due to extensive heating. Further, all the other peaks present in the XRD spectrum of untreated nanoclay were found unaltered even after thermal exposure. It is evident that, although water molecules were removed at higher temperature, as observed from IR data, the nanoclay maintained its structure. Therefore, the intrinsic properties of nanoclay remain unaltered even after extensive thermal exposure. Hence, the enhancement in the various properties of polymer matrix can be expected after incorporation of TMMT nanoclays.

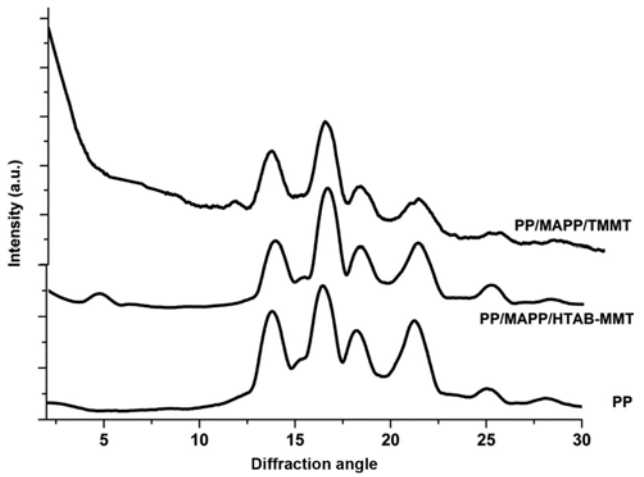

Fig. 3. XRD pattern of PP and its nanocomposites.

To investigate the morphology and crystalline structure, XRD diffractograms of the PP and nanocomposites were analyzed and represented in Fig. 3. We noticed that the peak corresponding to the d-spacing of nanoclay was shifted from higher (2θ=6.9; d_{001}= 1.4 nm) to the lower diffraction angle (2θ=5; d_{001}=1.6 nm) in the case of nanocomposites reinforced with Na-MMT (PP/MAPP/Na-MMT). However, the corresponding d_{001} peak in case of TMMT nanoclay reinforced polymer nanocomposites (PP/MAPP/TMMT) completely disappeared, revealing the possible exfoliation of clay layers in polymer matrix [23]. This may be a result of strong interaction between polar groups of MAPP molecules and unsaturated oxygen present in silicate layers, developed due to dehydroxylation [24, 25]. Hence, XRD pattern formation of possible exfoliated structure of in PP/MAPP/TMMT nanocomposites was evident, whereas negligible degree of intercalation in case of untreated clay reinforced PP matrix. The effect of Na-MMT and TMMT on the crystalline morphology of PP matrix was also evaluated by WAXD in the range of 10-30^0 (Fig. 3). A slight difference in the intensities of peak α (110) and α (040) was observed for neat PP and both the nanocomposites. But no shift was noticed in the peak position, indicating the unaffected typical crystalline pattern after incorporation of unmodified and modified nanoclay. The intensity of the peaks in WAXD pattern for PP/MAPP/TMMT was found slightly reduced with a slight broadening, as compared to that of PP/MAPP/Na-MMT. However the reduction in the intensity was not significant. And the estimated crystallinity of PP/MAPP/TMMT was found slightly higher than that of PP/MAPP/Na-MMT, which may result in improved mechanical properties of PP/MAPP/TMMT. Any traces of presence of β crystals were not noticed after incorporation of nanoclay. This result indicates that the crystal type of PP did not change, that is, PP remained as a monoclinic crystal type. The mean crystallite size was determined by the perpendicular direction of hkl plane using the following equation:

$$L_{hkl}=[(K\lambda)/(B\cos\theta_{hkl})] \quad (1)$$

Following, Scherrer equation, the mean crystallite size (L) was determined in the perpendicular direction of hkl plane using Eq. (1). K

Table 1. Micro-structural properties of PP and its nanocomposites

Material/Variable	Orientation index		Mean crystallite size (nm) with respect to different planes		
	A_{110}	A_{040}	L_{110}	L_{040}	L_{130}
PP	0.53	0.41	10.5	14.2	16
PP/MAPP/Na-MMT	0.51	0.49	10.7	14.7	16
PP/MAPP/TMMT	0.74	0.47	11.2	14.7	16

is the crystallite shape constant (=0.89), λ is the wavelength of CuK_α radiation, $B=(b_{hkl}^2-b_0^2)^{1/2}$, where b_{hkl} is the full width middle height (FWHM) of the peak for the (hkl) reflection and b_0 the instrumental resolution determined from the LaB6 reference sample and is the diffraction angle. Crystallite size, L_{040} perpendicular to the 040 planes and mean crystallite size, t, perpendicular to the plane corresponding to the clay platelet surface were evaluated. The results obtained from the XRD analysis are represented in Table 1. There was a slight increase, noticed in the crystallite sizes perpendicular to the plane (110) and (040). Whereas unaltered crystallite size was observed for that of the perpendicular to (130) crystal plane. This is attributed to the presence of a foreign entity, in this case nanoclay, which may have induced some PP crystallite orientation without any change in crystallite size [26]. This observation was in accordance with the results reported earlier [27].

Hence, without using organic chemicals the nanoclay can be exfoliated and dispersed uniformly in PP matrix in order to achieve the synergistic properties of clay and polymer.

3. Mechanical Properties

To evaluate the mechanical performance accurately, tensile properties of the nanocomposites were determined and represented in Table 2. Tensile properties such as tensile strength at yield, Young's modulus, percentage of elongation at break for PP and its nanocomposites were investigated. Ductile behavior was observed in all cases. Incorporation of unmodified Na-MMT exhibited decrease in tensile strength. This was attributed to the low aspect ratio of clay platelets and low contact surface area, leading to lower tensile properties. In addition, this may also be attributed to the filler-filler interaction, leading to formation of agglomerates, induced local stress concentration hence reduced tensile properties [28]. This supported the fact that no particle-polymer interaction could be achieved in PP/MAPP/Na-MMT. Hence, an incoherent nature of clay particle with PP matrix was observed [29]. This led to the formation of stress concentration effect in some region and to the early fracture. Higher Young's modulus and tensile strength of PP/MAPP/TMMT as compared to neat PP was noticed. This is because of exfoliated clay layers inside the PP matrix, because the level of intercalation/exfoliation is the responsible factor for improvement in mechanical properties [30]. This is because the delamination of nanoscale clay particles in the matrix restricts the mobility of polymer chains under loading [31,32]. Orientation of clay platelets and polymer chains with respect to the loading direction may also contribute to the reinforcement effect. Also, it leads to the occurrence of high contact area between polymer chain and clays, which enables strong interaction between PP (modified with MAPP) chains and clay layers. Also, as expected the compatibilizer acted as a bridge or buffer for the formation of interlock points between polymer chain and clay platelets and resulted in improved material stiffness [33]. The strong interaction between TMMT layers and PP/MAPP matrix can be explained as follows. The major effect of dehydroxylation relates to the octahedral sheet, wherein, "residual" oxygen remains behind in the dehydroxylated structure (this is a high temperature phase that develops topotactically from low temperature form). Octahedrally coordinated cations in the low-temperature form become five coordinated cations in the dehydroxylated structure, with the maintained topological features. Upon dehydroxylation, the two associated OH groups in the low temperature form react to form an H_2O molecule, which leaves the structure and one residual oxygen, which moves to the position midway between, which was formerly the OH---OH, shared edge of the octahedral in the low temperature form. The residual oxygen remains much unsaturated with respect to the positive charge and requires a compensation for the disruption of local charge neutrality. When this unsaturated residual oxygen comes in contact with the polar group of PP/MAPP, a strong interaction is probably achieved to compensate the charge neutrality [25].

Hence, from the improved modulus and strength of PP/MAPP/TMMT nanocomposites, it was evident that, in case of PP nanocomposites reinforced with TMMT nanoclay, the uniform nanometric dispersion of silicate layers, in matrix had been taken place. This is due to strong interaction between TMMT layers and PP/MAPP matrix and delaminated clay layers due to effect of steam build up [21]. This leads to the improved interfacial stress transfer efficiency and extent of induced deformation, as a result of strong bonding between filler and matrix [34]. Hence, the stiffness of silicate layers contributes to the presence of immobilized or partially immobilized polymer phases [35].

The impact properties of PP and its nanocomposites were also investigated. To maintain the accuracy of the results five specimens were tested. From the observation it is evident that the impact strength of PP/MAPP/Na-MMT nanocomposite was lower as compared to neat PP. This is attributed to the restricted mobility of polymer chains due to agglomeration of the clay particles in the PP matrix. Agglomeration of these particles limits the utilization of intrinsic properties of these fillers along with polymer matrix. These agglomerates clay particles act as initial crack and then reduce the impact toughness

Table 2. Mechanical properties of Polypropylene nanocomposites

Specimen label	Tensile stress at yield (MPa)	Tensile strain at yield (%)	Modulus (MPa)	Impact strength (J/m)	Elongation at break
PP	30±1	8.2±0.2	983±6	41±0.7	>500
PP/MAPP/Na-MMT	33±2	6.8±0.5	1179±4	40±0.4	>500
PP/MAPP/TMMT	37±2	7.11±0	1444±5	50.1±2	>500

[36].

However, the relatively higher impact strength by 25%, of the PP/MAPP/TMMT nanocomposites, as compared to neat PP, revealed the uniform dispersion and exfoliation [37] of TMMT layers, resulting in platelet structure and relative anisotropy. This might also be attributed to the nucleating effect of TMMT clay, leading to the increase in the interface among spherulites and preventing the development of cracks in matrix, resulting in improved toughness and impact strength of matrix polymer. The nucleating effect of TMMT might be ascribed to the highly delaminated and uniformly dispersed TMMT layers, hence providing a higher number of nucleating sites inside the PP/MAPP matrix (since the foreign particles inside the polymer matrix act as nucleating sites for crystallization). This supports the good toughening effect of TMMT nanoclay, which acts as efficient crack stopper and forms a tortuous crack propagation path, resulting in higher impact strength of PP matrix [38]. Therefore, from the highest mechanical properties of the PP/MAPP/TMMT, it may be concluded that the thermally induced dehydroxylation of nanoclay may be an efficient method to achieve the synergism between PP and nanoclay.

On the other hand, this improvement in the stiffness and strength of the nanocomposites by adding TMMT occurs without any reduction of the elongation at break of the material.

4. Heat Deflection Temperature (HDT)

Nanofiller proposed here increases the heat-distortion temperature of polymers. The heat deflection temperature for PP and its nanocomposites PP/MAPP/Na-MMT and PP/MAPP/TMMT has also been investigated and reported in Fig. 4. From the analysis, the deflection temperature for the nanocomposites was much higher than the virgin PP. As compared to virgin PP, the increase in HDT value was 1.6% and 19.7%, respectively. This is attributed to the very uniform nano-dispersion of MMT in a polymer matrix, leading to uniform stress distribution. Uniformly dispersed fillers create tie points between crystallites, bridging the amorphous phase and causing it to soften above its glass-transition temperature [39]. The increase in HDT due to TMMT dispersion is an important improvement for PP from both industrial and application viewpoint, since it is difficult to achieve HDT enhancement by modification or reinforcement of filler. The improvement of HDT originates from the mechanical stability of the nanocomposites, compared to the neat PP, rather any increase of polymer melting point. Therefore, the increased HDT value for the PP nanocomposites revealed the enhanced mechanical stability as compared with neat PP [40]. This also supports the findings obtained from mechanical property analysis in previous sections. Hence, the increased thermo-mechanical property (i.e., HDT) of PP/MAPP/TMMT is ascribed to homogeneous and exfoliated morphology as compared to that of the PP/MAPP/Na-MMT.

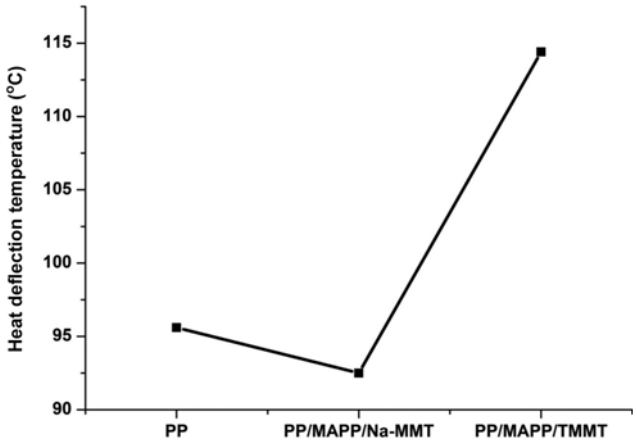

Fig. 4. Heat deflection temperature of PP and its nanocomposites.

5. Differential Scanning Calorimeter Analysis (DSC)

Differential scanning calorimeter is most convenient for analyzing the first-order transitions like melting and crystallization. Hence, to analyze the effect of dehydroxylated nanoclay on these transitions, samples were subjected to the DSC analysis in the temperature range of (−50 °C) to (300 °C) with a scanning rate of 10 °C/min. The results are presented in Table 3.

In all cases two cycles were recorded and the thermal characteristics were always evaluated from the second one in order to erase any previous thermal history of the sample. From the investigation, a slight increase in the heat enthalpy of PP nanocomposites was clearly observed as compared to that of neat PP. Similar observations have been recorded in case of organically modified clay reinforced nanocomposites [41].

Degree of crystallinity was obtained according to Eq. (2). The percent crystallinity of PP/MAPP/Na-MMT was found to be unaltered with respect to the neat PP. However, the relatively higher percent crystallinity was noticed in the case of PP/MAPP/TMMT nanocomposites as compared to neat PP and PP/MAPP/Na-MMT. This finding was in accordance with the WAXD analysis. This may be ascribed to the nucleating effect of TMMT clay, which favors crystallization by providing a higher degree of the nucleation density [42]. Hence, it can be reasoned that the nucleating effect of nanoclay was significantly enhanced after dehydroxylation. This agreed with the observation for impact property analysis of this study.

$$Xc = \frac{\Delta H_m}{f_p \Delta H_m^0} \times 100 \quad (2)$$

However, the melting point of both the nanocomposites was shifted towards the slightly lower temperature (3% as compared to that of neat PP). A similar observation was noticed in case of organophilized clay-reinforced nanocomposites [27,42]. Melting and crystallization peak of the nanocomposites remained unaltered after incorporation of Na-MMT. This is attributed to the unexfoliated morphology of the nanocomposites [41]. However, the onset for the melting; $\mathbf{T_{m\,(onset)}}$,

Table 3. Melting and crystallization behavior of the PP and its nanocomposites

Material	T_m (°C)	$T_{m(onset)}$ (°C)	$T_{c(onset)}$ (°C)	$T_{c(end)}$ (°C)	T_c (°C)	% X_c
PP	175.5	123.8	119.3	110.2	88.1	55
PP/MAPP/Na-MMT	169.45	123.6	120.8	111.7	90.3	55.7
PP/MAPP/TMMT	169.66	142.4	127.1	120	103.9	61

was shifted towards the higher temperature in the case of PP/MAPP/TMMT. This improvement of the onset melting temperature was greater by 6% as compared to that of neat PP. This revealed the improved thermal stability of the polypropylene with the incorporation of TMMT nanoclays. The melting peak of PP was broader as compared to nanocomposites, revealing the asymmetric wing towards lower temperature; however, the narrow peak of PP/MAPP/TMMT nanocomposites [12] supports the nucleation effect of TMMT clays, which in turn may have caused the improved crystallinity of the polypropylene. Therefore, the reduction in the melting temperature range may be a subsequent effect of the narrowed distribution of crystal dimension and improved crystallinity in case of PP/MAPP/TMMT [43].

Furthermore, the crystallization behavior of the PP and its nanocomposites showed an improvement in the crystallization temperature **(T_c)** after incorporation of TMMT clay. The onset temperature of crystallization $\mathbf{T}_{c(onset)}$ and the end crystallization temperature, $\mathbf{T}_{c(end)}$, was shifted towards the higher temperature. These advances in the crystallization temperature revealed the reinforcing effect of nanoclays, which might have resulted in the improved crystallinity of the PP matrix. The reinforcing effect on crystallization temperature was not evident in PP/MAPP/Na-MMT nanocomposites.

Thermal stability of the nanocomposites can also be observed using DSC analysis, by determining the degradation onset temperature, which is represented by the onset of oxidation processes that leads to thermal degradation [44]. Wherein, the oxidation onset temperature for PP was at 227 °C, which was slightly shifted (4 °C) towards higher temperature in the case of the PP/MAPP/Na-MMT. The oxidation onset of PP/MAPP/TMMT was drastically higher than PP and PP/MAPP/Na-MMT as shown in Fig. 5. This increase

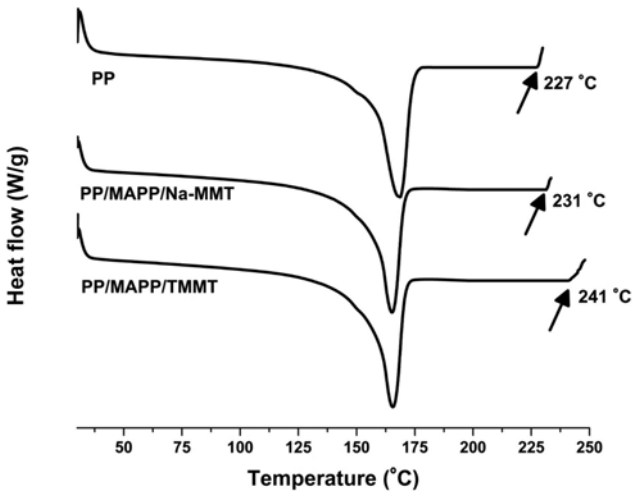

Fig. 5. DSC thermogram of PP and its nanocomposites.

was almost 13 °C higher than that of neat PP, revealing the efficiency of TMMT in improving the thermal stability of polymer nanocomposites. This observation is in accordance with the finding of reported earlier [44].

6. Thermogravimetric Analysis (TGA)

The extremely interesting properties of polymer clay nanocomposites are its thermal stability and unparalleled power to promote flame retardancy through the formation of insulating and incombustible char [41].

The thermal stability of the PP and its nanocomposites with Na-MMT and TMMT clay has been assessed. The degradation temperature at different stages has been observed and reported in the Table 4. The different temperature, which has been reported, is $\mathbf{T}_{d(0.1)}$: Temperature for 10% weight loss, $\mathbf{T}_{d(0.5)}$: Temperature for 50% weight loss, $\mathbf{T}_{d(0.95)}$: Temperature for 95% weight loss, $\mathbf{T}_{d(onset)}$: Onset temperature for degradation, $\mathbf{T}_{d(end)}$: Onset temperature for degradation, and $\mathbf{T}_{d(max)}$: Peak temperature for the degradation. The $\mathbf{T}_{d(0.1)}$ and $\mathbf{T}_{d(0.5)}$ represent the initial thermal stability of the material [45].

From the analysis, it was evident that the temperatures $\mathbf{T}_{d(0.1)}$ and $\mathbf{T}_{d(0.5)}$ were shifted towards higher temperature for both nanocomposites, which might be attributed to the reinforcing effect of the nanoclay that results in the formation of char layer. Wherein the increase in the $\mathbf{T}_{d(0.1)}$ and $\mathbf{T}_{d(0.5)}$ value of PP/MAPP/Na-MMT was very less significant. Whereas, a drastic increase of $\mathbf{T}_{d(0.1)}$ and $\mathbf{T}_{d(0.5)}$ by 14% and 7% was noticed in PP/MAPP/TMMT as compared to neat PP, revealing the improved initial thermal stability of the PP/MAPP/TMMT. This is in accordance with the results reported earlier [12].

However, the $\mathbf{T}_{d(0.95)}$ for the Na-MMT reinforced nanocomposites are lower than that of virgin PP which is attributed to the instability of char layers at high temperature and therefore also start degrading as polymer matrix as well as to the un-delaminated clay morphology in nanocomposites. The $\mathbf{T}_{d(0.95)}$ of PP/MAPP/TMMT was higher than that of virgin PP, which might be ascribable to the thermal stability of the treated clay at higher temperature, since it has been already exposed to higher temperature, leading to the thermo-insulating effect of thermally treated clay with polymer matrix [21].

The onset temperature of degradation, $\mathbf{T}_{d(onset)}$, of the PP/MAPP/Na-MMT and PP/MAPP/TMMT, nanocomposites was also shifted towards the higher temperature by 1% and 26%, respectively, indicating the much higher thermal stability of PP/MAPP/TMMT as compared to neat PP as well as to the PP/MAPP/Na-MMT nanocomposites. However, a different trend was noticed for $\mathbf{T}_{d(end)}$ where the $T_{d(end)}$ for PP/MAPP/Na-MMT was lower than that of neat PP. However, $T_{d(end)}$ value of PP/MAPP/TMMT was much higher than that of neat PP and PP/MAPP/Na-MMT. The shift in the degradation temperature towards the higher side is attributed to the formation of a high performance carbonaceous silicate char that gets built up on the surface, insulating the underlying material and slowing the

Table 4. Thermal degradation temperature of the PP and its nanocomposites

Material	$T_{d(0.1)}$ (°C)	$T_{d(0.5)}$ (°C)	$T_{d(0.95)}$ (°C)	$T_{d(onset)}$ (°C)	$T_{d(end)}$ (°C)	$T_{d(max)}$ (°C)
PP	362.3	410.6	435	311	426	459
PP/MAPP/Na-MMT	367.4	412.5	422	315	421	427
PP/MAPP/TMMT	413.3	439.5	457	394	446	465

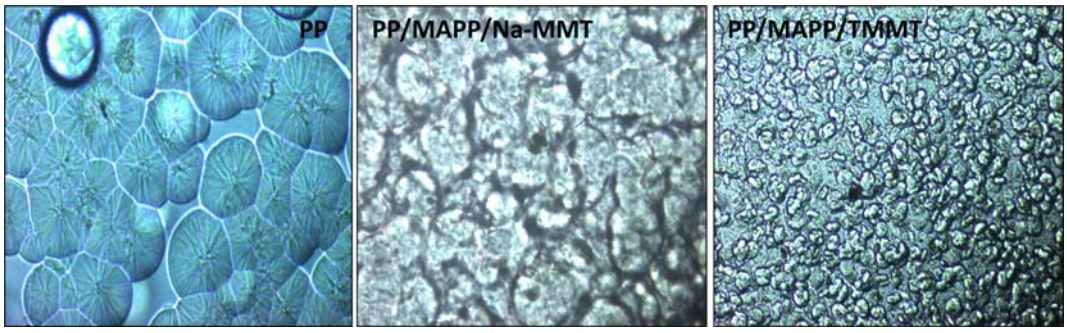

Fig. 6. Optical microscopic images of PP and its nanocomposites (scale: 100 μm).

degradation and escape of volatile products generated during decomposition [41].

The peak temperature $T_{d(max)}$ of the PP/MAPP/Na-MMT was lower than that of virgin PP, which might be attributed to the loss of semicrystalline morphology during degradation step. Also, it suggested that the char layer formed, which is the responsible factor in the shifting of weight loss curves, was not stable at high temperature and therefore it degraded as polymer matrix. This observation also supports the presence of un-exfoliated structure. Most of the organophilic-treated nanoclay reinforced PP nanocomposites have been reported to have lower $T_{d(max)}$.

However, the peak temperature of the PP/MAPP/TMMT nanocomposites was noticeably higher as compared to the polymer matrix. This might be due to the greater thermal stability of the thermally treated clay at higher temperature, which is a result of thermo-insulating properties of the TMMT clay (TMMT) achieved through extensive thermal exposure [21].

The weight loss of the clay occurs due to the residual water present in it [41]. However, in case of TMMT, the clay is devoid of residual water since it is dehydroxylated at higher temperature. This provides the possibility of higher thermal stability to the polymer/clay nanocomposites, because the important factor of clay degradation (residual water) has been already removed. This observation was completely different from the observation reported earlier about PP nanocomposites reinforced with organically treated nanocomposites, where the thermal stability at higher temperature and peak degradation temperature was found lower than neat PP due to the products developed during the degradation reaction of surfactant (e.g., Hofmann reaction) [11]. However, the presence of side products, formed during decomposition of PP/MAPP/TMMT, is enormously reduced due to the absence of any chemical-based surfactant.

To investigate the thermal stability of PP and its nanocomposites, the activation energy of the materials was computed according the integral kinetic equation of Horowitz-Metzger equation method (Eq. (3)).

$$\ln[\ln(1-\alpha)^{-1}] = E_a\theta/RT^2 \tag{3}$$

where α is the weight loss, $\theta = T - T_{d(max)}$

The estimated values of the activation energy for PP/MAPP/Na-MMT and PP/MAPP/TMMT were 93 and 115 kj/m^2, respectively, which was greater than 90 kj/m^2 value of neat PP. Hence, from this observation, the thermal stability of the PP/MAPP/TMMT nanocomposites is significantly higher as compared to that of neat PP. This is in accordance with the concept of greater stability of the thermally modified MMT at higher temperature. Since the decomposable component (residual water), which is imparted in the decomposition reaction, of the MMT has been already excluded from heat treatment of the material. Hence the analysis of activation energy exhibits a similarity with the findings obtained in the previous discussion of analysis of TGA data.

7. Optical Microscope

Fig. 6 represents optical microscopic images of PP and its nanocomposites. PP has a four leaf clover pattern when it is crystallized. In case of PP/MAPP/Na-MMT, non-uniform distribution of spherulites was noticed, which is due to non-uniformly dispersed Na-MMT inside the PP matrix, and the spherulite size in this case was slightly reduced, but the change was virtually negligible.

Unlike PP, PP/MAPP/TMMT nanocomposites exhibited a rod-like scattering pattern; this was ascribed to the arrangement of radiating primary lamellae. The uniformly distributed spherulites in PP/MAPP/TMMT revealed the uniformly dispersed clay layers in PP matrix. The spherulite size was drastically reduced in the case of PP/MAPP/TMMT as compared to that of PP, revealing the efficient nucleating effect of TMMT on PP matrix. The primary nucleation density of the spherulites, (N) can be calculated using Eq. (4) considering uniform sizes of spherulites.

$$N = \left(\frac{3}{4\pi}\right)(D_m/2)^{-3} \tag{4}$$

where D_m is the maximum diameter of the spherulite, i.e., the attainable diameter before impingement [45]. The primary nucleation density of PP, PP/Na-MMT and PP/MAPP/TMMT was found to be 5.36×10^{-6}, 10.13×10^{-6} and 3.4×10^{-5}, respectively. The high nucleation density of the nanocomposites exhibited more nucleation sites at the same time. Hence, it is evident that the nucleation site was higher in the case of PP/MAPP/TMMT, revealing the uniform distribution of TMMT layers inside the PP matrix.

8. Transmission Electron Microscope (TEM)

To correlate the morphological results obtained by XRD and DSC analysis, we analyzed the transmission electron microscopic images of the nanocomposites. The TEM micrographs of the PP/MAPP/Na-MMT and PP/MAPP/TMMT are in Fig. 7. The clay particles in the micrographs are indicated by dark areas and the gray region represents the continuous PP matrix. TEM micrographs of the PP/MAPP/Na-MMT nanocomposites revealed the presence of agglomerates of clay layers inside the clay matrix. However, PP/MAPP/

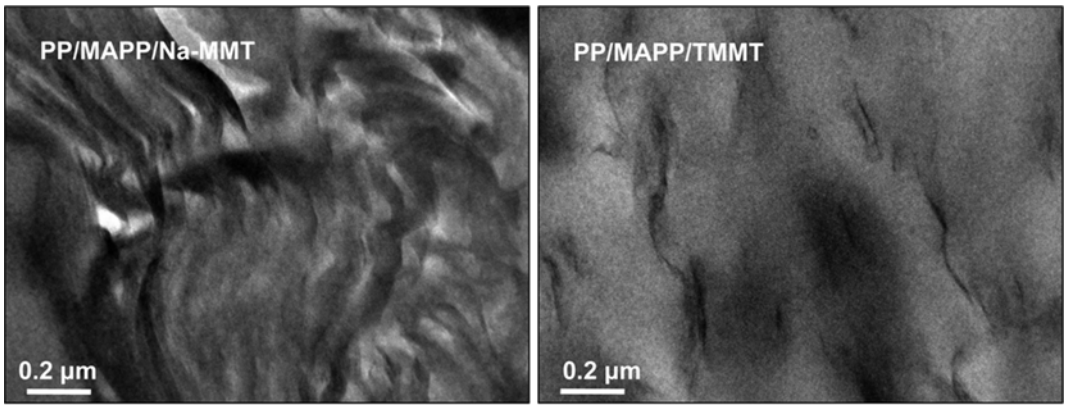

Fig. 7. TEM micrographs of nanocomposites.

Table 5. Flammability properties of Polypropylene (PP) and its nanocomposites

Specimen label	Time to ignition (TTI) (sec)	Peak HRR (kW/m^2)	Average mass loss rate (g/s)
PP	30	871	0.070
PP/MAPP/Na-MMT	23	826	0.087
PP/MAPP/TMMT	25	537	0.070

TMMT nanocomposite had a more uniform dispersion of the nanoclay layers within the PP matrix as compared to the PP/MAPP/Na-MMT nanocomposites. Higher degree of delamination of clay layers was observed in PP/MAPP/TMMT nanocomposites. The agglomerates observed in the PP/MAPP/Na-MMT nanocomposites were absent in PP/MAPP/TMMT hybrids. This phenomenon is attributed to the improved interaction of clay layers and polymer matrix, which facilitated the separation of stacks from each other, thereby resulting in homogeneous distribution within the matrix polymer.

9. Cone Calorimeter Analysis

To evaluate the fire retardant properties, a combustion analysis of the PP and its nanocomposites was performed with a cone calorimeter experiment; the result is in Table 5. In case of neat PP at the end of the test no residue was left, revealing the poor carbonization of PP [47]. No significant change in the time to ignition (TTI) was noticed for PP and its nanocomposites, which was in accordance with the results reported by Jash and Wilkie [48], revealing that the time required to burn the entire surface with a luminous flame for PP and both the nanocomposite systems does not show considerable difference.

Fig. 8 shows the heat release rate (HRR) of the PP and its nanocomposites. The lowest HRR value of the PP/MAPP/TMMT nanocomposites as compared to PP and PP/MAPP/Na-MMT revealed the much higher flame retardant behavior of TMMT fillers as compared to Na-MMT. Furthermore, a much lowered peak heat release rate (PHRR) was observed for PP/MAPP/TMMT as compared to PP and PP/MAPP/Na-MMT. A decrease in PHRR indicates a reduction of burnable volatiles generated by the degradation of a polymer matrix; such a drop clearly indicated the flame retardant effect of network structure created between TMMT particles and their "molecular" distribution throughout the matrix. This supports the

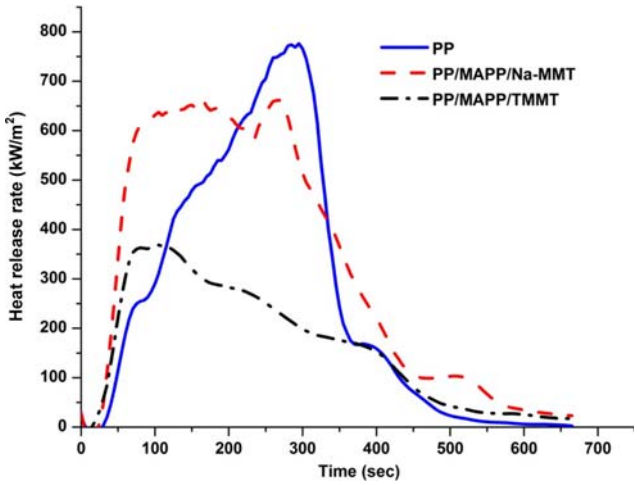

Fig. 8. (a) Mass loss rate vs time, (b) heat release rate vs time; of PP and its nanocomposites.

highly delaminated clay layers of TMMT, inside the polymer matrix, and strong interaction between clay layers and PP/MAPP. The interaction between dehydroxylated clay and polymer is ascribed to the unsaturated oxygen present in silicate layers, developed due to dehydroxylation [24,25]. This was in accordance with the previous observations of this study.

Average mass loss rate (AvMLR) is another important defining factor in determining the fire-retardant property. The AvMLR of PP/MAPP/Na-MMT was higher than that of neat PP, revealing the catalytic effect of clay in enhancing the flammability of polymer due to the presence of burnable volatiles. However, the AvMLR for PP/MAPP/TMMT was similar to that of PP. This can be ascribed to the absence of burnable volatiles in TMMT, hence reducing the catalytic activity of clay in increasing the flammability.

The weights of samples before and after combustion were observed, wherein the percentage of weight loss on the ignition of PP/MAPP/TMMT was less than that of the PP/MAPP/Na-MMT [49]. This might be due to the presence of some moieties in Na-MMT; for example, in the form of free radicals (due to the presence of water molecules) which get burned and cause comparatively more weight loss. However, the low weight loss of TMMT was attributed to the absence of any such type of free radical moieties, which further con-

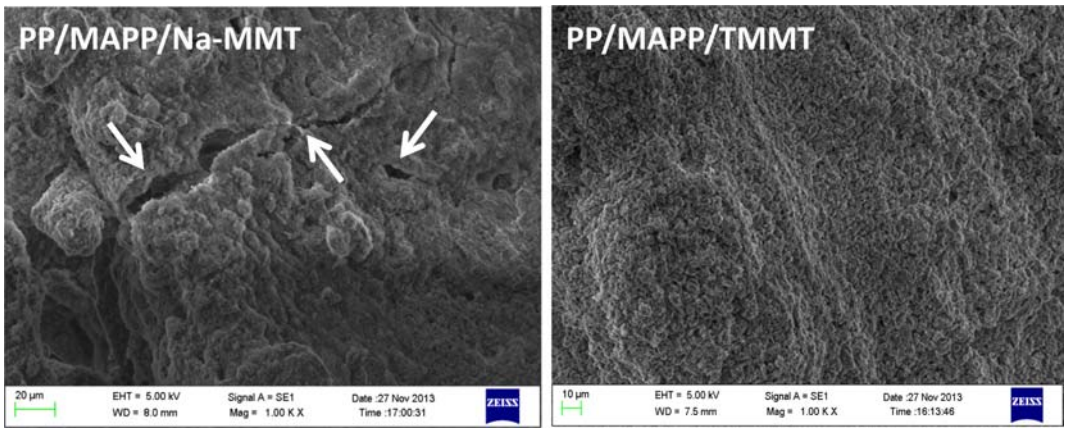

Fig. 9. SEM micrographs of burned residues after cone calorimeter test (a).

firms the insulating behavior of thermally dehydroxylated clay [21].

10. Scanning Electron Microscope (SEM)

Fig. 9 represents the SEM micrographs of the char residue obtained after the cone calorimeter test. The SEM micrograph of the residue obtained after burning of nanocomposites showed the formation of a tight protective char on the surface, which blocks the thermal wave from penetrating down the surface. A carbonaceous layer was also found to cover whole surface of the sample. However, in case of the PP/MAPP/Na-MMT a crack in the char layers was noticed, unlike for PP/MAPP/TMMT. This opening in the char layer might be due to the bubbles evolving from the interior of the sample, which push away the platelets to form openings throughout the layer. Formation of the bubbles is ascribed to the presence of free radicals formed due to heating of water molecules present in the clay layers. However, the absence of crack in the char of PP/MAPP/TMMT revealed the absence of free radicals, leading to better insulating capability. This agreed with the cone calorimeter observations. Hence, the removal of water molecules from the clay layers, through dehydroxylation, leads to enhanced flame retardant characteristics of clay.

CONCLUSION

A new, chemical-free method to modify the interfacial adhesion between clay and polymer matrix has been developed through dehydroxylation of the clay via extensive heating. To validate the successful modification and its influence on polymer, various properties were analyzed. An improvement in the mechanical properties revealed the applicability of this modification for polymer nanocomposite applications. The enhanced properties of polymer matrix were confirmed using WAXD analysis, from which the successful formation of the exfoliated structure was evident in PP/MAPP/TMMT. Improved crystallization and thermal stability of the PP/MAPP/TMMT nanocomposites was also in accordance with the morphological observations. The nucleating effect of the TMMT nanoclay on the spherulitic structure was clearly evident from the optical microscopic images. The highly delaminated morphology of PP/MAPP/TMMT was further confirmed by transmission electron microscopic analysis. The combustion analysis showed much improved flame retardant property and much delaminated layers of thermally dehydroxylated clay (TMMT) as compared to untreated clay (Na-MMT). Also, the SEM micrographs of the char residue obtained after cone calorimeter experiment revealed better insulating properties of TMMT as compared to Na-MMT.

From the all studied aspects of PP/MAPP/TMMT nanocomposites it can be concluded that the interface between clay and polymer can be successfully modified by avoiding the use of organic chemicals, via the extensive heating and quenching of the nanoclay. This prevents users from having to handle hazardous chemicals in order to achieve the exfoliated morphology in polymer nanocomposites.

TABLE OF NOMENCLATURE

PP : polypropylene
FTIR : fourier transform infrared spectroscopy
WAXD : X-ray diffraction
MAPP : maleic anhydride grafted polypropylene
Na-MMT : montmorillonite nanoclay
TMMT : thermally treated (dehydroxylated) montmorillonite nanoclay
TEM : transmission electron microscopy
HDT : heat deflection temperature
TGA : thermogravimetric analysis
PP/MAPP/Na-MMT : PP nanocomposites reinforced with Na-MMT
PP/MAPP/TMMT : PP nanocomposites reinforced with TMMT
$\mathbf{T}_{d(0.1)}$: temperature for 10% weight loss
$\mathbf{T}_{d(0.5)}$: temperature for 50% weight loss
$\mathbf{T}_{d(0.95)}$: temperature for 95 % weight loss
$\mathbf{T}_{d(onset)}$: onset temperature for degradation
$\mathbf{T}_{d(end)}$: onset temperature for degradation
$\mathbf{T}_{d(max)}$: peak temperature for the degradation
N : nucleation density
$\mathbf{D}_m$: maximum spherulite diameter

REFERENCES

1. M. Alexandre and P. Dubois, *Mater. Sci. Eng.*, **28**, 1 (2000).
2. E. P. Giannelis, *Adv. Mater.*, **8**, 29 (1996).

3. S. G. Lei, S. V. Hoa and M. T. Thon-That, *Compos. Sci. Technol.*, **66**, 1274 (2006).
4. M. Y. A. Fuad, H. Hanim, R. Zarina, Z. A. M. Ishak and A. Hassan, *Exp. Polym. Lett.*, **4**, 611 (2010).
5. S. S. Ray and M. Okamoto, *Prog. Polym. Sci.*, **28**, 1539 (2003).
6. W. Gianelli, G. Ferrara, G. Camino, G. Pellegatti, J. Rosinlhal and R. C. Trombini, *Polym.*, **46**, 7037 (2005).
7. X. Liu and Q. Wu, *Polym.*, **42**, 10013 (2001).
8. H. Y. Yao, J. Zhu, A. B. Morgan and C. A. Wilkie, *Polym. Eng. Sci.*, **42**, 1808 (2002).
9. A. Nese, S. Sen, M. A. Tasdelen, N. Nugay and Y. Yagci, *Macromol. Chem. Phys.*, **207**, 820 (2006).
10. L. Cui, D. M. Khramov, C. W. Bielawski, D. L. Hunter, P. J. Yoon and D. R. Paul, *Polymer*, **49**, 3751 (2008).
11. V. Mittal, *Thermally stable flame retardant polymer nanocomposites*, Cambridge University Press, United Kingdom (2011).
12. K. Chrissopoulou, I. Altintzi, I. Andrianaki, R. Shemesh, H. Retsos, E. P. Giannelis and S. H. Anastasiadis, *J. Polym. Sci.: Part B: Polym. Phys.*, **46**, 2683 (2008).
13. A. Chafidz, I. Ali, M. E. A. Mohsin, R. Elleithy and S. A. Zahrani, *J. Polym. Res.*, **19**, 9906 (2012).
14. C. O. Rohlmann, M. D. Failla and L. M. Quinzani, *Polym.*, **47**, 7795 (2006).
15. Z. Zhou, S. Wang, Lan Lu, Y. Zhang and Y. Zhang, *J. Polym. Sci. Part B: Polym. Phys.*, **45**, 1616 (2007).
16. S. Y. Lu and S. J. Kim, *J. Colloid Interface Sci.*, **248**, 231 (2002).
17. X. He, J. Yang, L. Zhu, B. Wang, G. Sun, P. Lv, I. Y. Phang and T. Liu, *J. Appl. Polym. Sci.*, **102**, 542 (2006).
18. M. L. López-Quintanilla, S. Sánchez-Valdés, L. F. Ramos de Valle and R. G. Miranda, *Polym. Bull.*, **57**, 385 (2006).
19. J. W. Lee, Y. T. Lim and O. O. Park, *Polym. Bull.*, **45**, 191 (2000).
20. M. A. Karakassides, D. Gournis and D. Petridis, *Clay Miner.*, **34**, 429 (1999).
21. F. Bergaya, B. K. G. Theng and G. Lagaly, *Handbook of clay science*, Elsevier, Amsterdam (2006).
22. V. Khunova and Z. Zamorsky, *Polym.-Plas. Technol. Eng.*, **32**, 289 (1999).
23. S. Mohanty and S. K. Nayak, *Polym. Compos.*, **28**, 153 (2007).
24. I. Szazdi, A. Abranyi, B. Pukanszky and G. J. Vancso, *Macromol. Mater. Eng.*, **291**, 858 (2006).
25. A. F. Koster Van Groos and S. Guggenheim, *Am. Mineral.*, **74**, 627 (1989).
26. W. Xu, G. Liang, W. Wang, S. Tang, P. He and W-Ping Pan, *J. Appl. Polym. Sci.*, **88**, 3225 (2003).
27. L. Raka, G. Bogoeva-Gaceva and J. Loos, *J. Therm. Anal. Calorim.*, **100**, 629 (2010).
28. K. Zhang, L. Wang, F. Wang, G. Wang and Z. Li, *J. Appl. Polym. Sci.*, **91**, 2649 (2004).
29. D. A. D'Amico, L. B. Manfredi and V. P. Cyras, *Thermochim. Acta*, **544**, 47 (2012).
30. C. Marco, G. Ellis, M. A. Gomez and J. M. Arribas, *J. Appl. Polym. Sci.*, **88**, 2261 (2003).
31. F. Dogan, *Polypropylene*, InTech. Sd., Croatia (2012).
32. M. Naffakh, Z. Martin, C. Marco, M. A Gomez and I. Jimenez, *Thermochim. Acta*, **472**, 11 (2008).
33. L. G. Furlan, C. I. Ferreira, C. Dal Castel, K. S. Santos, A. C. Mello, S. A. Liberman, M. A. S. Oviedo and R. S. Mauler, *Mater. Sci. Eng. A*, **528**, 6715 (2011).
34. Z. Navrátilová, P. Wojtowicz, L. Vaculíková and V. Šugárková, *Acta Geodyn. Geomater.*, **147**, 59 (2007).
35. M. A. Karakassides, D. Gournis and D. Petridis, *Clay Miner.*, **34**, 438 (1999).
36. W. Liu, S. V. Hoa and M. Pugh, *Compos. Sci. Technol.*, **65**, 2364 (2005).
37. Kusmono, M. W. Wildan and Z. A. Mohd. Ishak, *Int. J. Polym. Sci.* (2013).
38. A. B. Inceoglu and U. Yilmazer, *Polym. Eng. Sci.*, **43**, 661 (2003).
39. J. Garcés, D. J. Moll, J. Bicerano, R. Fibiger and D. G. McLeod, *Adv. Mater.*, **12**, 1839 (2000).
40. E. Manias, A. Touny, L. Wu, K. Strawhecker, B. Lu and T. C. Chung, *Chem. Mater.*, **13**, 3516 (2001).
41. E. Olewnik, K. Garman and W. Czerwinski, *J. Therm. Anal. Calorim.*, **101**, 323 (2012).
42. B. K. G. Theng, *Formation and properties of clay-polymer complex*, Elsevier, Amsterdam (1979).
43. E. M. Araujo, R. Barbosa, C. R. S. Morais, L. E. B. Soledade, A. G. Souza and M. Q. Vieira, *J. Therm. Anal. Calorim.*, **90**, 841 (2007).
44. J. Pascual, E. Fages, O. Fenollar, D. Garcia and R. Balart, *Polym. Bull.*, **62**, 367 (2009).
45. C. Ding, D. Jia, H. He, B. Guo and H. Hong, *Polym. Test.*, **24**, 94 (2005).
46. S. Benerjee, M. Joshi and A. K. Ghosh, *J. Appl. Polym. Sci.* (2013), DOI:10.1002/App.39590.
47. H. Ma, L. Tong, Z. Xu and Z. Fang, *Nanotechnol.*, **18**, 375602 (2007).
48. P. Jash and C. A. Wilkie, *Polym. Degrad. Stab.*, **88**, 401 (2005).
49. P. K. Sahoo and R. Samal, *Polym. Degrad. Stab.*, **92**, 1700 (2007).